Efficient Electrochemical Performance of MnO_2 Nanowires interknitted Vanadium Oxide Intercalated Nanoporous Carbon Network as Cathode for Aqueous Zinc Ion Battery

Rimsha Mehek[1], Naseem Iqbal[1*], Tayyaba Noor[2], Yuanshen Wang[3] Alexey Y. Ganin[3]

[1]US-Pakistan Centre for Advanced Studies (USPCAS-E), National University of Sciences and Technology (NUST), H-12, Islamabad 44000, Pakistan.

[2]School of Chemical and Materials Engineering (SCME), National University of Sciences and Technology (NUST), H-12, Islamabad 44000, Pakistan.

[3]School of Chemistry, University of Glasgow, Glasgow, G128QQ, UK.

*Corresponding Author: Tel: +92 51 9085 5281, Email: **naseem@uspcase.nust.edu.pk**.

Abstract

Rechargeable aqueous Zn-ion batteries (AZIBs) have emerged as promising large-scale energy storage devices because of their low cost and good safety characteristics. Vanadium oxide-based materials have been actively studied as future cathode materials for AZIBs, benefiting from their suitable voltage and high specific capacity. However, poor rate performance and capacity deterioration due to the instability of their oxides is still a hurdle in their commercialization. Herein, we attempted to test a methodology involving the carbonization of V-MIL-101 to prepare a composite material consisting of vanadium oxide nanoparticles embedded within the nanoporous carbon network, which remarkably enhances the electrochemical performance of the material as a cathode in an aqueous Zn-ion battery system. The manganese oxide loading further stabilized the composite material, which improved the cathode material's rate capability in aq. zinc ion battery cathode. The cathode material MnO_2@NVC composite exhibited the capacity of 299 $mAhg^{-1}$ at 0.1C rate for 100 cycles benefitting from the synergistic effect of the high conductivity of Vanadium oxide nanoparticles and suitable voltage of MnO_2. The materials showed superior capacity retention and better cycling performance than unmodified vanadium oxide nanoparticles on carbon substrate as cathode material. The comparative morphological and electrochemical studies confirm the improved performance, which suggests that the vanadium oxide nanoparticles anchored on a high surface area carbon network intertwined with manganese oxide nanowires provide enhanced conductivity.

Keywords: Zinc Ion Battery, Manganese Oxide, Vanadium Oxide, Nanoporous Carbon

Introduction

Renewable energy sources have received much attention as a viable and practical solution to climate change. However, using renewable energy sources such as wind and solar demands the development of safe, cost-effective, and efficient energy storage systems capable of handling the volatility of renewable electricity production and consumer demand [1]. Aqueous Li-ion batteries are an attractive solution, but the scarcity of lithium supplies and using corrosive electrolytes is a further issue [2]. Therefore, Li-ion batteries are not suitable for large-scale energy storage in the long term [3, 4]. Cheaper and more abundant alternatives are needed, and aqueous zinc ion batteries have emerged as a practical solution to storing excess electricity. Copper hexacyanoferrate [5], V_2O_5 [6, 7], and MnO_2 [8, 9] are among the most promising electrodes for AZIBs.

Vanadium-based cathode materials have achieved a great deal of attention in this regard. The multiple oxidation states of vanadium have always made it a preferred choice in catalytic and redox reactions. Although vanadium oxides have shown considerably good discharge capacities in metal ion batteries, their commercialization still needs to be improved due to capacity deterioration even after a few cycles. Therefore, the vanadium oxide-based cathode needs modification and stabilization to be tested as a cathode for zinc ion batteries. The metal-organic framework has proved its strength as a precursor to synthesize carbonized metal oxide active material through pyrolysis. Thus, making a vanadium-based metal-organic framework with a suitable organic linker around it can result in a very sophisticated network-type structure with vanadium oxide-based nanoparticles embedded into a thin layer of nanoporous carbon substrate provides better stability and improved conductivity. Even though some progress may be obtained through this strategy, the capacity fading over high-rate long-term cycling performance can still be unsatisfactory due to structural degradation by complicated phase transitions upon Zn^{+2} insertion/extraction.

MnO_2 also stands out among cathode materials due to its substantial theoretical capacity (308 mA h/g) [10] and low cost of production. Zn-MnO_2 alkaline batteries have been retailed for a long time as single-use primary batteries [11]. The weak reversibility of MnO_2 in alkaline electrolytes prevents the building of rechargeable Zn-MnO_2 batteries [12-14]. Recent studies on the reversible insertion of Zn^{2+} into a MnO_2 host in an aqueous electrolyte have garnered attention as they could help design rechargeable Zn-MnO_2 batteries. It has been reported that various manganese dioxide phases, including spinel-type MnO_2, α-MnO_2, β-MnO_2, and γ-

MnO_2, could serve as host materials for Zn^{2+} ion in an aqueous electrolyte[15, 16]. Irrespective of the MnO_2 polymorph used, significant structural changes occur upon cycling processes that cause the MnO_2 host to delaminate into layered manganese oxide phases containing interlaminar water molecules[17, 18]. The dissolution of manganese from the structure and the introduction of hydrated Zn^{2+} (*i.e.*, $[Zn(H_2O)_6]^{2+}$) is believed to be responsible for the instability. These coordinated water molecules can effectively diminish the strong electrostatic repulsions between Zn^{2+} and the host material[19]. Theoretically, the layered structure with an extended interlayer spacing should be advantageous for storing guest-hydrated cations. However, a considerable volumetric shift causes a significant capacity fading throughout the phase-change process (*i.e.*, from α-, β-, γ-phase to layered structure with interlaminar water)[20].

Additionally, the layers of manganese oxide are disrupted during the charge/discharge process when hydrated cations are inserted, which perpetuates capacity fading. As a result, MnO_2 electrodes often display poor stability when cycled with high charge/discharge depth. To the best of our knowledge, it is the first time anyone has documented the steady cycling of a MnO_2-based electrode. Liu's group has obtained 84% of theoretical capacity (260 $mAhg^{-1}$) up to 45 cycles for MnO_2 in an aqueous electrolyte[21]. Recently, Chen et al. showed an improved cyclic life of 150 cycles with a 75% capacity retention (230 $mAhg^{-1}$)[22]. The stability of more than 5000 cycles has been attained with only a tiny percentage of the potential MnO_2 capacity being used (30%)[23]. Utilizing a MnO_2 cathode's large capacity effectively in an aqueous electrolyte is still risky. As was already stated, the capacity fading in the MnO_2 cathode occurs due to phase transition and the instability of the layered structure with H_2O intercalation. A possible strategy to strengthen the extended layered design is to use the MnO_2 in a host-guest composite structure as an electrode material which can minimize phase transitions[24].

Herein, a two-step synthesis methodology is applied to create the MnO_2 nanowires integrated within the nanoporous vanadium carbon (NVC) network. MnO_2 nanowires within the network of vanadium nanoparticles embedded within the nanoporous carbon structure effectively promote charge storage and strengthen the MnO_2 system. Thus MnO_2-anchored on NVC displays high-rate capability and long cycle life as prepared. Moreover, the ability of the MnO_2-wire type structures to intercalate H+ along with the Zn^{+2} and the presence of vanadium oxide nanoparticles within the nanoporous carbon structure stabilizes the overall composite cathode structure. The composition of host-guest chemistry between the NVC network and MnO_2 nanowires effectively promotes charge storage by avoiding irreversible phase transition. Thus, as-prepared MnO_2-intercalated NVC exhibits high-rate capability and long cycling life. The MnO_2-intercalated NVC nevertheless exhibited a highly stable cycling behaviour, which is better than earlier studies, with consumption even higher than 96% (299 $mAhg^{-1}$).

Experimental

Synthesis of V-MIL-101: Stoichiometric amounts (1:1 molar rations) of 2-Amino Terephthalic Acid (1.99 g) and Vanadium Chloride (VCl_3) (1.88 g) was dissolved in 60 mL of absolute ethanol. The well-dissolved mixture was sonicated for 15-20 mins and then transferred into a Teflon-lined autoclave. The autoclave was placed in an oven at 120°C for 48 hrs. The reaction mixture obtained was kept at room temperature for cooling before filtration. The precipitates were washed with ethanol and separated by centrifugation. The collected sample was vacuum dried at 70^{o}C overnight[25]. The prepared MOF material was labelled as MIL-101 (V).

Synthesis of NVC: After proper characterization, the prepared and thoroughly dried metal-organic framework was further pyrolyzed at 900^{o}C in a ceramic boat inside a tube furnace with a flowing N_2 gas atmosphere. The temperature ramp was set at 5^{o}C per minute, and the sample was kept at 900^{o}C for five hours. After the pyrolysis, the sample was washed with ethanol to clear the pores and vacuum dried at 70^{o}C for 4 hours to obtain a vanadium oxide-supported nanoporous carbon structure[26], labelled as NVC-900.

Synthesis of MnO_2@NVC: MnO_2 was synthesized within the nanoporous vanadium intercalated carbon network. The obtained NVC was washed and dried to eliminate all the water and other particulates entrapped within the pores. Then the NVC was impregnated with $Mn(NO_3)_2{\cdot}4H_2O$ solution corresponding to the 5 wt. % loading on the NVC. Afterward, the

above mixture was then ultrasonicated at 50°C for 1 h and dried in an oven at 70°C for 24 h. Finally, the dried samples were calcined in a tube furnace at 300 °C for 3.5 h under an inert atmosphere. The thus obtained MnO_2 nanowires intertwined on the nanoporous vanadium oxide intercalated carbon structure were denoted as MnO_2@NVC.

Results and Discussions

Characterization

To understand the conditions of pyrolysis required to convert the compact structure of V-MIL-101 into a high surface area porous carbon structure with VO embedded in it, the thermal profile of V-MIL-101 was obtained via thermogravimetric analysis (TGA). The thermal profile of the MOF precursor is shown in fig. 1(a) shows an initial loss of mass up to about 8.07%, which can be associated with the unreacted reactant species and water molecules stored within the voids of the metal-organic framework. Onwards until 900°C, a significant mass loss of about 44.6% occurs due to the breakage of compact construction and conversion into a porous structure. This information helps to determine the suitable pyrolysis temperature for converting V-MIL-101 into a sophisticated carbonized system with vanadium oxide nanoparticles embedded in it up to 900°C.

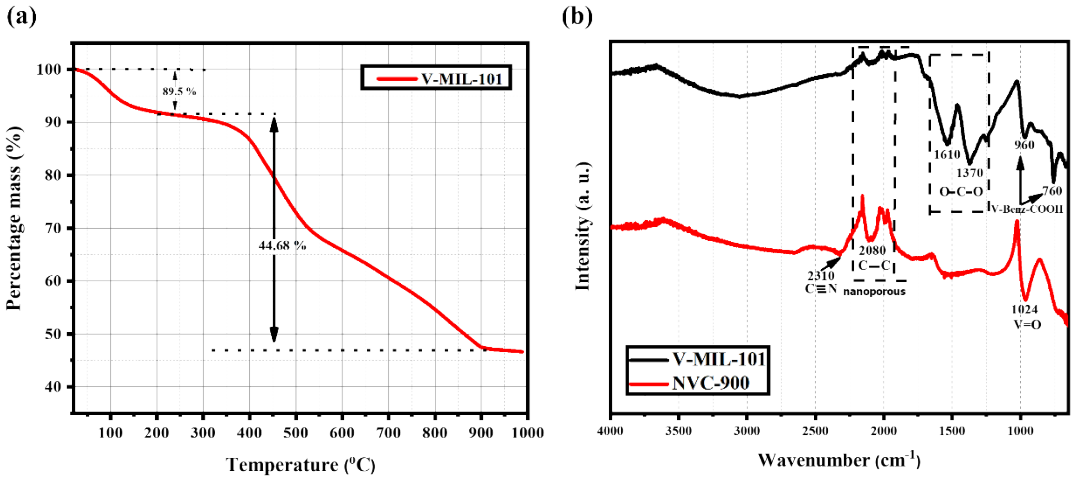

Figure 1. (a) Thermogravimetric profile of V-MIL-101 at temperature up to 1000°C (b) Fourier Transformation Infrared Spectrum of V-MIL-101 and vanadium oxide intercalated nanoporous carbon structure (NVC) obtained by pyrolysis of V-MIL-101

Fourier transform infrared (FT-IR) spectroscopy was used to analyze the functional groups present within the structure before and after the pyrolysis. Fig. 1(b) represents the functional

group bands in both structures[27, 28]. The V-MIL-101 structure shows strong bands of O-C=O from terephthalic acid at wavenumber values of 1610 and 1370 cm-1, along with sharp but small bands of V-COOH at 960 and 760 cm^{-1}. Upon pyrolysis at 900^{o}C, the C-C band at 2080 cm^{-1} is stronger, whereas the O-C=O bonds and V-COOH bonds deformed to make a nanoporous structure of carbon atoms. The V-O band at 1024 cm^{-1} is relatively straightforward, which can be attributed to the formation of vanadium oxide nanoparticles within the system.

The synthesis of MnO_2-intercalated NVC composite structure from scratch could be identified by the powder X-ray diffraction (XRD) pattern (Figure 2). The successful synthesis of V-MIL-101 can be confirmed by comparing it with the simulated powder pattern of Cr-MIL-101, which is the most reliable standard for MIL-101 structure[29]. The simulation was done by the CIF file using the Mercury software. All the peaks in V-MIL-101 match properly with the Cr-MIL-101, which shows that the V in V-MIL-101 is synthesized with the same chemistry as that of Cr in Cr-MIL-101[30]. The pyrolysis of this metal-organic framework structure resulted in the formation of fine powder with nano porosity homogenously distributed through the network of the carbon structure. The hkl value of (100) belongs to the graphitic carbon structure obtained by this method. On the other hand, the peaks with hkl values of (012), (104), (110), (113), (024), and (116) are due to the formation of vanadium oxide nanoparticles (JCPDS No: 85-1411) in the structure whereas the peaks with hkl values of (122), (214) and (300) majorly belong to the vanadium carbon bonding in the network[26, 31]. The XRD pattern after the in-situ composite formation of nanowires of MnO_2 (JCPDS NO: 81-2261) within this nanoporous carbon structure generated four identifying peaks at 2-theta values of 29 ^{o}, 37 ^{o}, 41^{o,} and 44^{o} with hkl values of (110), (101), (111) and (211) respectively[32].

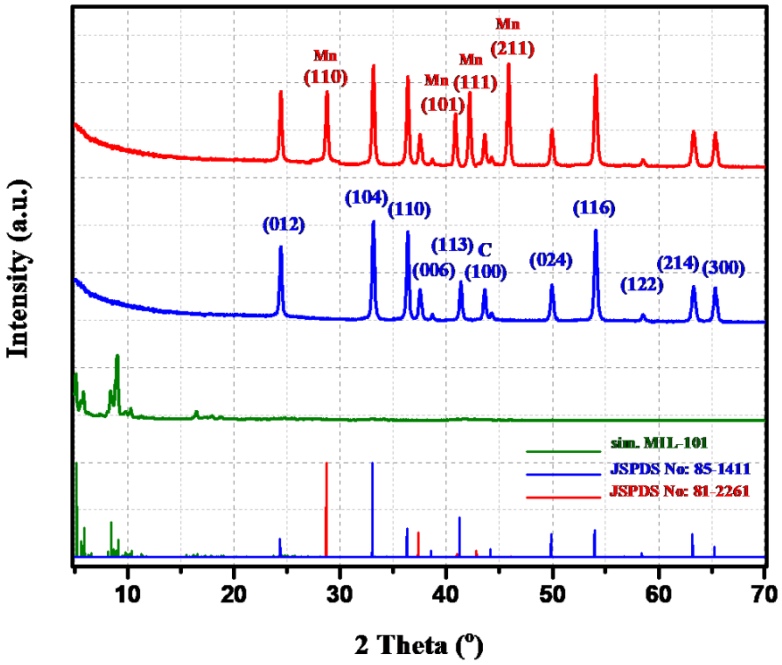

Figure 2. Powder diffraction pattern of V-Mil-101, NVC, and MnO2@NVC

The overall morphology of the synthesized composite has the host-guest type of chemistry where MnO_2 nanowires and nanoporous carbon structure combine as an interknitted sheath in which the vanadium oxide nanoparticles are embedded. The homogeneously distributed pores provide enhanced surface area with more active sites spread homogeneously over the cathode surface [26, 33]. This structure can be seen in the TEM images in fig 3(a), (b), and (c). The hexagonal nanostructures of vanadium oxide [34] can be seen submerged in the nanoporous carbon network. The HRTEM image of the same is also shown in figure 4(d). The composite of MnO_2-intercalated NVC can be visualized in fig 3 (e) and (f). The HRTEM of the MnO_2 nanowire [35] can be seen in Figures 3 (g) and (h). The nanowire has a typical width of less than 10 nm, whereas the characteristic carbon structure with vanadium species has an evenly distributed homogenous porosity. The TEM images reveal a MnO_2 nanowire-based knitted sheath-like structure attached to the nanoporous carbon structure with vanadium oxide nanocrystals embedded in them[24]. The carbon-vanadium network stabilizes the nanowires, making the structure significantly less likely to undergo irreversible phase transitions.

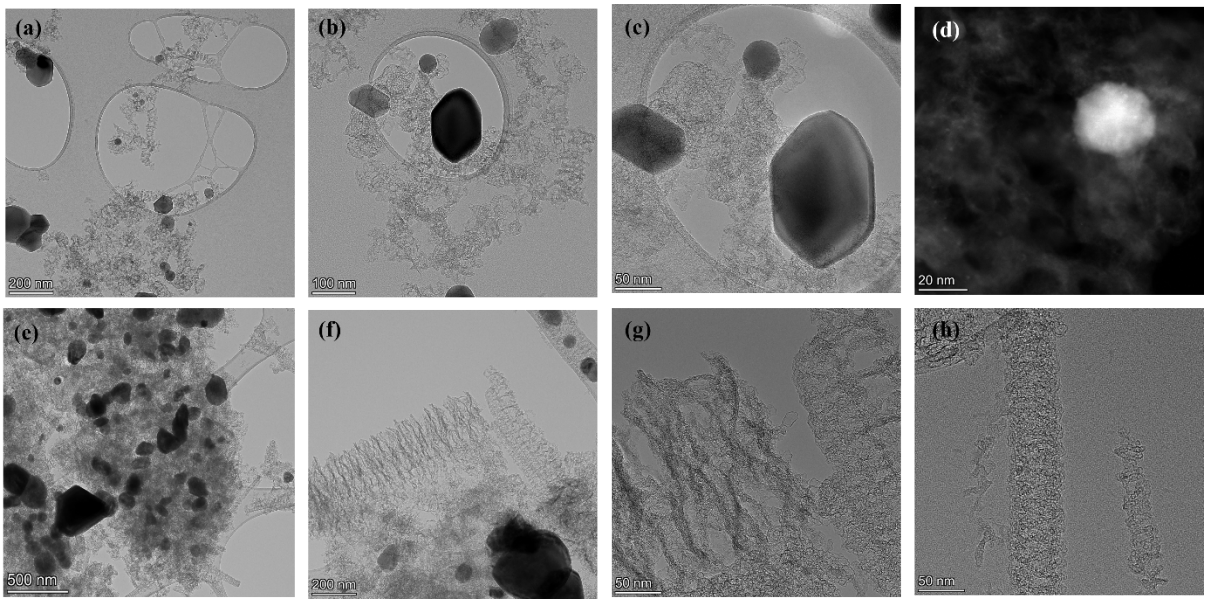

Figure 3. Transmission Electron Microscopy Images of (a-c) nanoporous vanadium carbon structure (d) HRTEM of VO nanoparticles embedded within the nanoporous carbon network (e-g) inter-knitted MnO2 nanowire within the nanoporous carbon vanadium structure (h) HRTEM of MnO_2 nanowire

The elemental mapping was performed via STEM-HAADF, where the carbon nanoporous structure's homogenous distribution with vanadium oxide is intercalated through it in figure 4 (a-c). On the other hand, the distribution of Manganese and oxygen, as in MnO_2, through the carbon network can be seen in figure 4 (d-f).

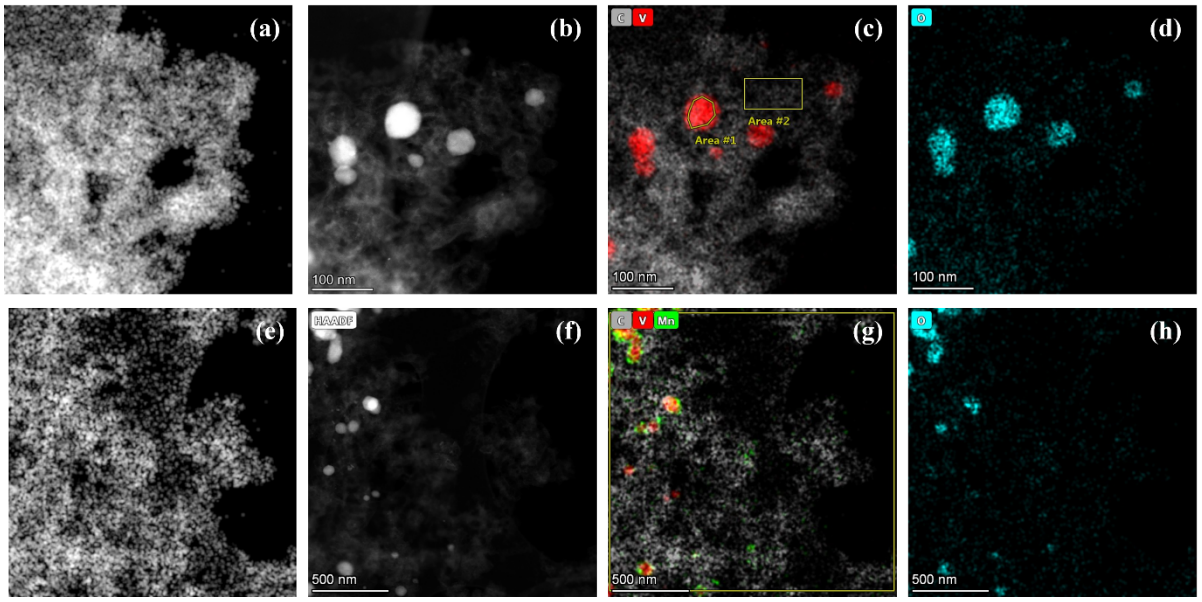

Figure 4. Elemental Mapping through STEM-HAADF showing the distribution of (a-d) Carbon, Vanadium, and Oxygen in NVC and (e-h) Carbon, Vanadium, Oxygen, and Manganese in MnO2@NVC

The homogenous distribution of all the elements confirms the successful knitted structure of the MnO_2 nanowires in the NVC network, where vanadium oxide nanoparticles can be seen embedded within the nanoporous carbon network in Figures 4 (a) and (b).

The nitrogen adsorption-desorption isotherm of V-MIL-101 in figure 5 (a) and (b) shows a vast surface area of 357 cm^3/g at STP and a pore size that is primarily centred at 7 nm to 13 nm, also clearly show a hysteresis loop, which further supports the porous structure[36]. After the pyrolysis of V-MIL-101, the nanoporous design was developed with an even higher surface area of 659 cm^3/g at STP, which is almost double the compact structure of the MOF precursor. The nanoporosity was achieved with a significant portion of pore size in the 10 nm range. This porous structure not only anchors the vanadium oxide species there but can also enhance the conductivity by facilitating charge transfer[33].

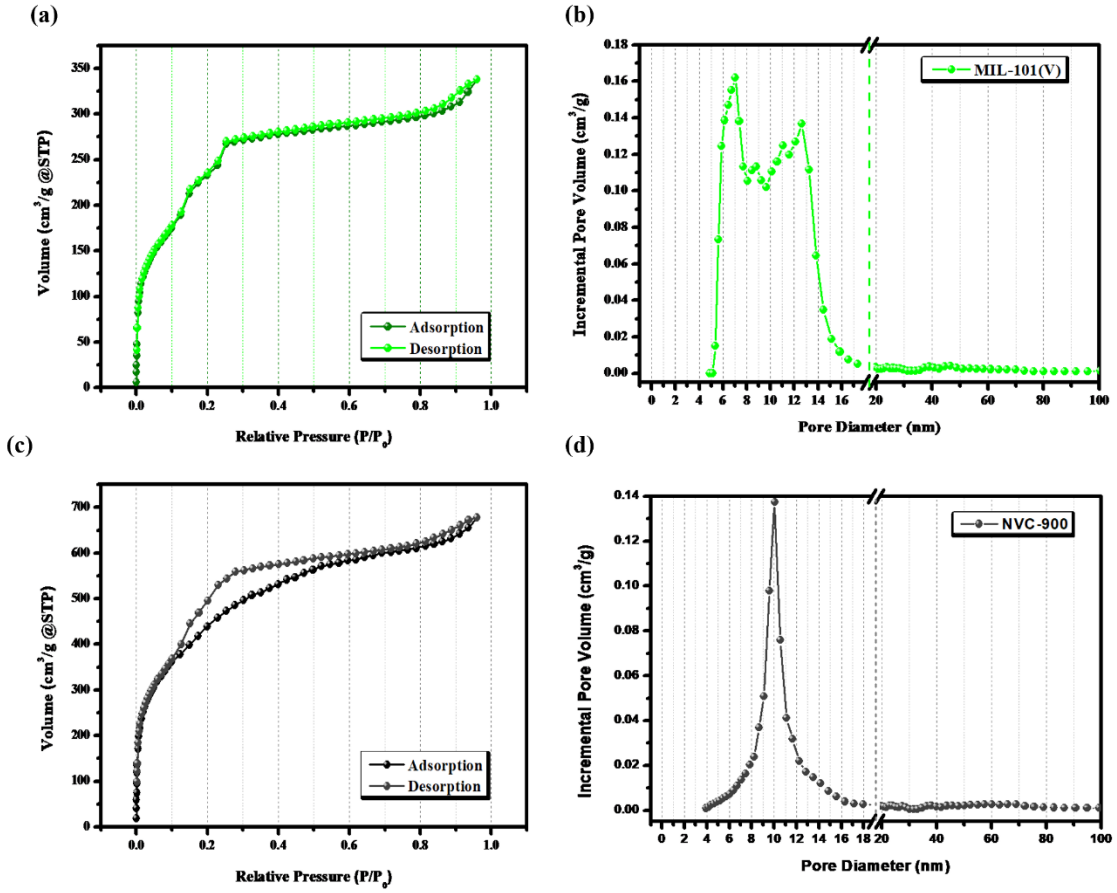

Figure 5. (a) N_2 adsorption-desorption isotherms of V-MIl-101 (b) Pore size distribution of V-MIL-101 (c) N_2 adsorption-desorption isotherms of nanoporous vanadium carbon (NVC) structure (d) Pore size distribution of NVC

To further analyze the structure of MnO_2@NVC, X-ray photoelectron spectroscopy (XPS) was performed to see the respective energies of orbitals involved in the bonding. The B.E spectrum of V2p in fig. 6(b) orbital shows a good intensity at B.E values at 515 eV for $V2p_{3/2}$ and 519 eV for $V2p_{1/2}$. The C1s peak fitting shows the formation of a carbon network with neighbouring carbon and oxygen atoms in fig. 6(c).

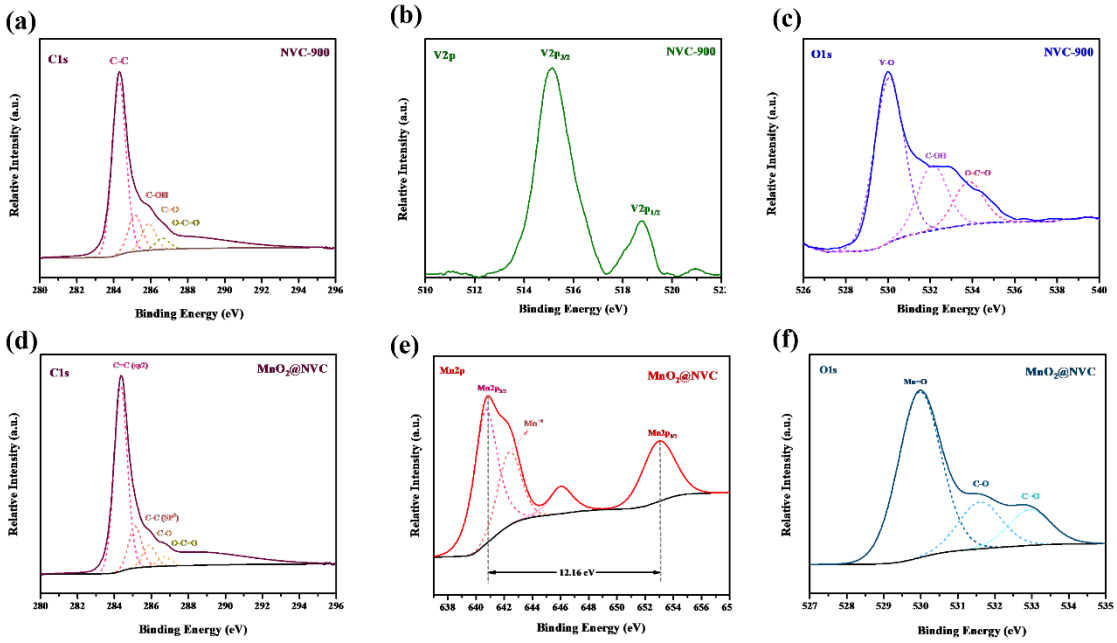

Figure 6. (a-c) XPS spectrum of NVC (d-f) XPS spectrum of MnO_2@NVC

Likewise, the C1s peak fitting in fig. 6(d) shows a shift of bonds from C-C to C=C (sp^2) due to the bonding with Mn^{+4} species. The spectrum in fig. 6(e) shows an intense peaks related to Mn2p fitted at BE value of 640.9 eV for $Mn2p_{3/2}$ and at 653.1 eV for $Mn2p_{1/2}$. These two peaks have a difference of 12.16 eV along with a shoulder peak related to Mn^{+4} in the MnO_2-intercalated NVC, suggesting a 4.0 charge state of Mn in the composite. The peak fitting of O1s further confirmed the bonding of Mn and O in MnO2 in MnO_2-intercalated NVC in fig. 6(f). The highest peak fitted in this case belongs to Mn=O, which confirms the successful intercalation of MnO_2 with the NVC structure[37, 38].

Electrochemical Characterization

The cyclic voltammetry (CV) results of as-synthesized vanadium MOF V-MIL-101 and the sample after the pyrolysis of V-MIL-101 at 900°C and after the loading of MnO_2 for the composite formation of MnO_2@NVC as cathode material for an aqueous zinc ion battery are displayed in Figures 7 and 8. The CV scans were taken at variable rates ranging from 0.1 to

1.0 mV/s. CV scans of V-MIL-101 and pyrolyzed NVC-900 at 1.0 mV/s are given in Figures 7 (a) and (b). Likewise, CV scans of MnO_2@NVC are shown in figure 8 (a) at scan rates of 0.1 to 1.0 mV/s. At every scan rate, two redox couples can be seen very clearly. At a scan rate of 1.0 mV/s, MnO_2@NVC shows the first oxidation peak can be seen at 0.67 V, and the second oxidation peak appears at 1.08 V. Similarly, at the same scan rate first reduction peak can be seen at potential 0.98 V, and the second reduction peak appears at potential 0.57 V. The insertion mechanisms of Zn^{2+} during the discharge process are responsible for the two-step charge storage. The two peaks represent the probability that the zinc ion can intercalate into the structure of the host material at two different sites[39].

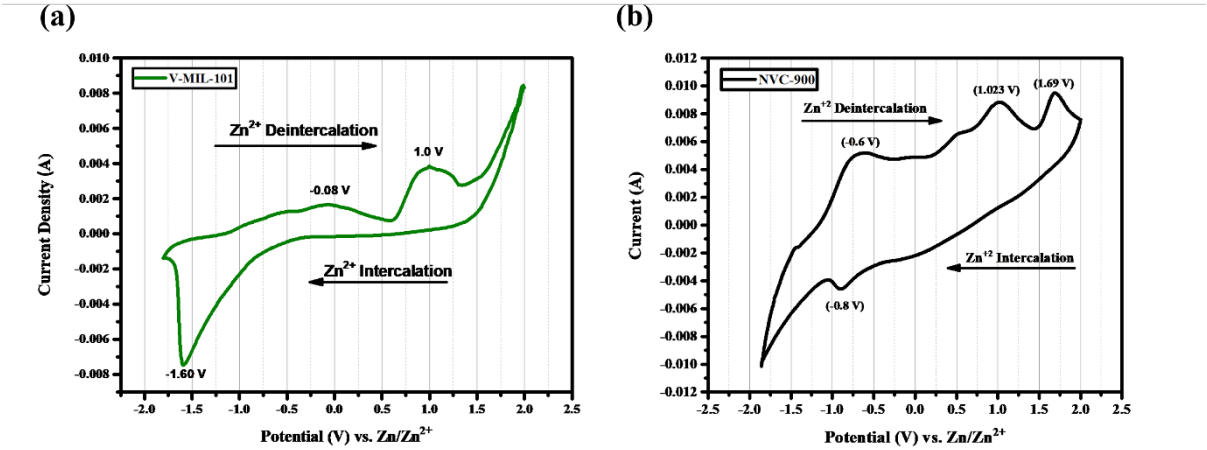

Figure 7. (a) Cyclic voltammogram of Vanadium metal-organic framework (V-MIL-101) at scan rate (b) Cyclic voltammogram of nanoporous vanadium carbon structure pyrolyzed at 900°C (NVC-900)

This can be further affirmed through the galvanostatic charge-discharge. The standard Swagelok-type cell, consisting of a MnO_2-intercalated NVC composite cathode, a Zn foil anode, and an aqueous electrolyte (1M $ZnSO_4$) adsorbed with a glass fibre separator, is used to describe the electrochemical profile of the MnO_2-intercalated NVC nanolayers composite. The MnO_2-intercalated NVC composite's galvanostatic charge/discharge profile is depicted in figure 7(b), where the obtained capacity and applied current density are determined by mass loading of the MnO_2@NVC as the cathode (i.e., 2 mg/cm^2 with a 1 cm^2 electrode area). The cell displays high initial discharge capacity when tested at a low current of 0.1 C, with two subsequent plateaus appearing in both the charge and discharge curves. The discharge capacity is increased to 299 mAhg^{-1} in the following cycle, nearly the theoretical capacity of 308 mAh/g. The first plateau appears between 1.08 V and 0.81 V potential vs. Zn/Zn^{+2}. The second

discharge plateau appears between 0.74 V and 0.57 V. The potential values of these plateaus match perfectly with the redox couples appearing on the cyclic voltammograms of this cathode material. These plateaus are not very flat in nature. Instead, the discharge curve seems quite sloppy. The slopy discharge curve appears because the cathode material doesn't undergo any irreversible phase transition during the deintercalation of zinc ions between the cathodic layers[40].

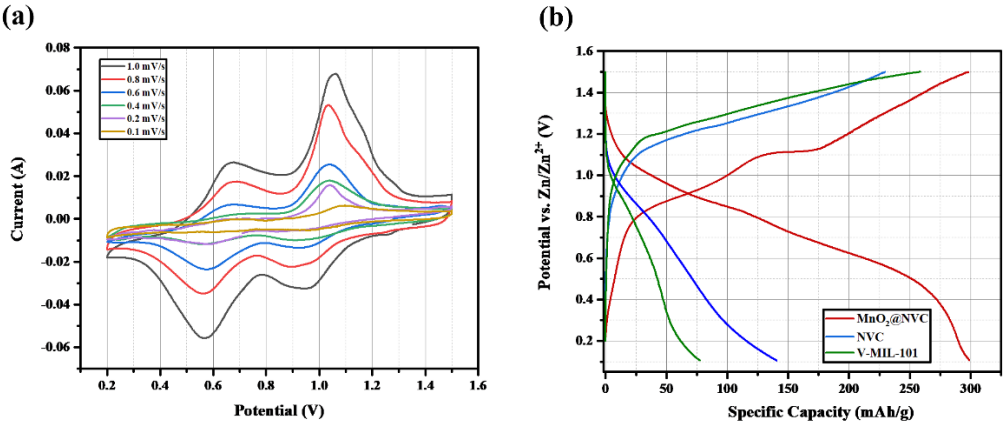

Figure 8. (a) Cyclic Voltammogram of MnO_2@NVC at variable scan rates between 0.1 mV/s an d1.0 mV/s at voltage range between 0.2V and 1.5V (b) Charge Discharge Profile of V-MIL-101, NVC and MnO_2@NVC between potential range of 0.2V to 1.5V at 0.1C

In the case of V-MIL-101, the discharge capacity drops even further to 77.68 mAh/g. V-MIL-101 and NVC show two plateaus in their discharge curves since the structure undergoes two phase transitions during two-step deintercalation. This increases the chance of irreversible structural deformation, leading to structural collapse and decreasing discharge capacity over the long-term cycling capacity. The small value of the discharge capacity of V-MIL-101 compared to the higher charge capacity can be attributed to the fact that the compact structure of V-MIL-101 is distorted during intercalation. The exact amount of zinc ions cannot be deintercalated during the discharge cycle, compromising the system's overall discharge capacity and reducing the cathode material's coulombic efficiency. Similarly, in the case of nanoporous carbon structure with vanadium oxide species, the discharge capacity is improved up to 140 mAh/g with a promising discharge pattern due to the high conductivity and better charge transfer in the NVC structure because of the increased surface area. To combat the high theoretical capacity for the zinc ion batteries, the NVC structure is further loaded with MnO_2 nanowires by the in-situ method. The loading of MnO_2 nanowires knitted through the

nanoporous carbon structure with vanadium oxide species creates a synergistic effect and results in a stable composite system of MnO_2@NVC.

The rate performance measured at various c-rates is shown in Figure 8(a), and rate capability up to 100 cycles is shown in figure 8(b). The cell displays a reversible discharge capacity of 283.1 $mAhg^{-1}$ at 1C, which is quite close to that at the low rate of 0.1C. After subsequent cycles up to c-rates as high as 10C, another run of 10 cycles at 1C still gives a discharge capacity of 272.6 mAh/g, which is among the most excellent rate performances recorded to date among various cathode materials for zinc ion batteries.

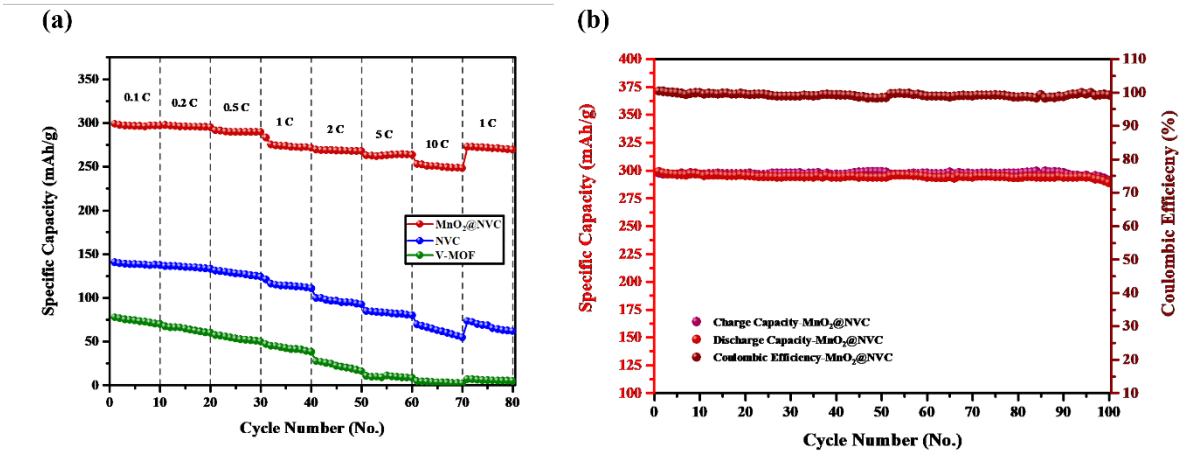

Figure 9 (a) Rate performance of V-MIL-101, NVC, and MnO_2@NVC at various C-rates between a low current density of 0.1C and a high current density of 10C. (b) Cyclic performance of MnO_2@NVC after 1st cycle of activation up to further 100 cycles of charge and discharge generating coulombic efficiency

At 0.1C, the MnO_2-intercalated NVC composite's cycle stability was assessed. Figure 8(b) shows that at the 100th discharge cycle, the discharge capacity of the MnO_2-intercalated NVC composite is 288.89 mAh/g. Therefore, it can be stated that the MnO_2@NVC has achieved an ultra-high utilization of more than 96% (based on the theoretical capacity of 308 mA h g1) for 100 cycles with coulombic efficiency averaging around 100%.

The electrochemically stable behaviour can also be analyzed via an EIS plot of all three structures. Figure 8 shows the decrease in charge transfer resistance (R_{CT}) as we move from a metal-organic framework structure to the nanofabrication and then to the loading of highly conductive MnO_2 nanowires into the structure.

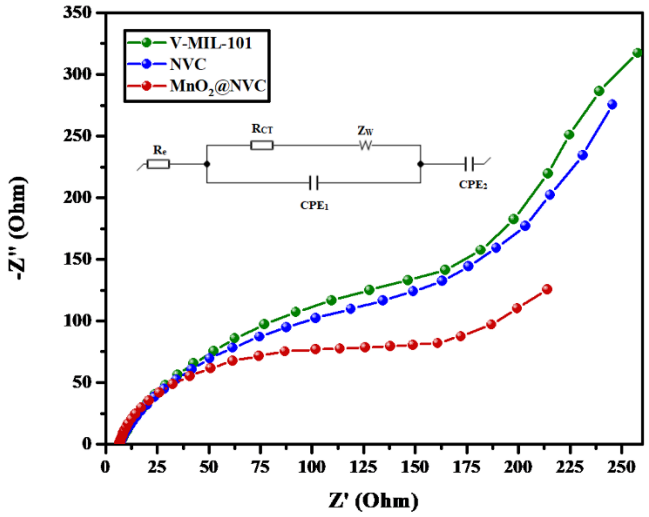

Figure 10. Nyquist plots of V-MIL-101, NVC, and MnO_2@NVC, and corresponding equivalent circuit

Reaction Mechanism

The reaction mechanism during cycling in neutral aqueous electrolytes is still being determined since manganese dioxide exists in various crystallographic polymorphs. Here a two-step intercalation and deintercalation process can be proposed based on the plots achieved in galvanostatic charge-discharge testing. During the intercalation, the H^+ from the aqueous electrolyte first intercalates into MnO_2@NVC nanolayers producing hydroxide species near the cathode. In contrast, the second charge platform appears due to a Zn^{2+} insertion process. As a result, we have two clear plateaus in the charge curve of the MnO_2@NVC cathode. Due to the presence of highly conductive vanadium transition metal in the structure anchored on the high surface area carbon nanoporous network with enhanced charge transfer capacity, the MnO_2 doesn't undergo any phase transitions. After charging, it doesn't dissolute into other side products of manganese with H^+ or OH^-. Therefore, our system doesn't see clear flat plateaus in discharging curves. This saves manganese from undergoing irreversible transitions after the charging, and the structure remains intact for the subsequent cycles. At the same time, more zinc hydroxide sulphate forms on the electrode surface due to the combination of zinc with free hydroxide ions. This "self-regulation function" eliminates extra OH, which is favourable for high cycle stability. The zinc hydroxide sulphate may dissolve upon recharge due to the released H^+[24].

Conclusions

In conclusion, MnO_2@NVC was synthesized and examined as the cathode material for a mild aqueous electrolyte rechargeable Zn-MnO_2 battery. The MnO_2-intercalated NVC exhibit improved rate performance and outstanding cycle stability at high charge/discharge level due to their characteristic nano size, spacious carbon network, homogeneously distributed nanosized porosity, and nanowire type interknitted reinforced layered structure of MnO_2. It is shown that the hydrated H^+/Zn^{2+}-insertion-induced phase transformation and the subsequent structure disintegration can be effectively eliminated by the vanadium oxide-reinforced nanoporous structure in combination with the nanosized (10 nm) MnO_2 structure. This is vital for achieving a long cycle life and high capacity uptake.

Acknowledgment

Higher Education Commission, Pakistan, financially supported this work. Experimental and Technical support by the School of Chemistry, University of Glasgow, and U.S.-Pakistan Centre for Advanced Studies in Energy is highly acknowledged.

References

1. Guo, Y.G., J.S. Hu, and L.J. Wan, *Nanostructured materials for electrochemical energy conversion and storage devices.* Advanced Materials, 2008. **20**(15): p. 2878-2887.
2. Huang, J., et al., *Progress of organic electrodes in aqueous electrolyte for energy storage and conversion.* Angewandte Chemie, 2020. **132**(42): p. 18478-18489.
3. Zhang, Y., P. Xin, and Q. Yao, *Electrochemical performance of $LiFePO_4$/C synthesized by sol-gel method as cathode for aqueous lithium ion batteries.* Journal of Alloys and Compounds, 2018. **741**: p. 404-408.
4. von Wald Cresce, A. and K. Xu, *Aqueous lithium-ion batteries.* Carbon Energy, 2021. **3**(5): p. 721-751.
5. Qiu, S., et al., *Prussian blue analogues as electrodes for aqueous monovalent ion batteries.* Electrochemical Energy Reviews, 2021: p. 1-21.
6. Li, Y., et al., *V_2O_5 nanopaper as a cathode material with high capacity and long cycle life for rechargeable aqueous zinc-ion battery.* Nano Energy, 2019. **60**: p. 752-759.
7. Qi, Z., et al., *Harnessing oxygen vacancy in V_2O_5 as high performing aqueous zinc-ion battery cathode.* Journal of Alloys and Compounds, 2021. **870**: p. 159403.
8. Ding, S., et al., *Oxygen-deficient β-MnO_2@ graphene oxide cathode for high-rate and long-life aqueous zinc ion batteries.* Nano-micro letters, 2021. **13**(1): p. 1-12.
9. Zhang, Y., et al., *MnO_2 cathode materials with the improved stability via nitrogen doping for aqueous zinc-ion batteries.* Journal of Energy Chemistry, 2022. **64**: p. 23-32.

10. Zhao, Y., Y. Zhu, and X. Zhang, *Challenges and perspectives for manganese-based oxides for advanced aqueous zinc-ion batteries.* InfoMat, 2020. **2**(2): p. 237-260.

11. Liu, X., et al., *Rechargeable Zn–MnO_2 batteries: advances, challenges and perspectives.* Nanotechnology, 2020. **31**(12): p. 122001.

12. Shin, J., et al., *A review on mechanistic understanding of MnO_2 in aqueous electrolyte for electrical energy storage systems.* International Materials Reviews, 2020. **65**(6): p. 356-387.

13. Faegh, E., et al., *Understanding the dynamics of primary Zn-MnO_2 alkaline battery gassing with operando visualization and pressure cells.* Journal of The Electrochemical Society, 2018. **165**(11): p. A2528.

14. Magar, B.A., et al., *Ab initio studies of discharge mechanism of MnO_2 in deep-cycled rechargeable Zn/MnO_2 batteries.* Journal of The Electrochemical Society, 2020. **167**(2): p. 020557.

15. Shi, W., W.S.V. Lee, and J. Xue, *Recent development of Mn-based oxides as zinc-ion battery cathode.* ChemSusChem, 2021. **14**(7): p. 1634-1658.

16. Dai, Q., et al., *The secondary aqueous zinc-manganese battery.* Journal of Energy Storage, 2022. **55**: p. 105397.

17. Wu, B., et al., *Graphene scroll-coated α-MnO_2 nanowires as high-performance cathode materials for aqueous Zn-ion battery.* Small, 2018. **14**(13): p. 1703850.

18. Fang, G., et al., *Suppressing manganese dissolution in potassium manganate with rich oxygen defects engaged high-energy-density and durable aqueous zinc-ion battery.* Advanced Functional Materials, 2019. **29**(15): p. 1808375.

19. Li, Y., et al., *Reaction mechanisms for long-life rechargeable Zn/MnO_2 batteries.* Chemistry of Materials, 2019. **31**(6): p. 2036-2047.

20. Uchaker, E., *Impact of Structure and Defect Modification on Vanadium Oxide for Alkali-ion Battery Electrodes*. 2015.

21. Pan, H., et al., *Reversible aqueous zinc/manganese oxide energy storage from conversion reactions.* Nature Energy, 2016. **1**(5): p. 1-7.

22. Zhang, N., et al., *Rechargeable aqueous zinc-manganese dioxide batteries with high energy and power densities.* Nature communications, 2017. **8**(1): p. 1-9.

23. Sun, W., et al., *Zn/MnO_2 battery chemistry with H^+ and Zn^{2+} coinsertion.* Journal of the American Chemical Society, 2017. **139**(29): p. 9775-9778.

24. Huang, J., et al., *Polyaniline-intercalated manganese dioxide nanolayers as a high-performance cathode material for an aqueous zinc-ion battery.* Nature Communications, 2018. **9**(1): p. 2906.

25. Carson, F., et al., *Framework Isomerism in Vanadium Metal–Organic Frameworks: MIL-88B(V) and MIL-101(V).* Crystal Growth & Design, 2013. **13**(11): p. 5036-5044.

26. Kim, J., N.D. McNamara, and J.C. Hicks, *Catalytic activity and stability of carbon supported V oxides and carbides synthesized via pyrolysis of MIL-47 (V).* Applied Catalysis A: General, 2016. **517**: p. 141-150.

27. Wang, Y., W. Guo, and X. Li, *Activation of persulfates by ferrocene–MIL-101 (Fe) heterogeneous catalyst for degradation of bisphenol A.* RSC advances, 2018. **8**(64): p. 36477-36483.

28. Surya Bhaskaram, D., R. Cheruku, and G. Govindaraj, *Reduced graphene oxide wrapped V_2O_5 nanoparticles: green synthesis and electrical properties.* Journal of Materials Science: Materials in Electronics, 2016. **27**(10): p. 10855-10863.

29. Shadmehr, J., S. Zeinali, and M. Tohidi, *Synthesis of a chromium terephthalate metal organic framework and use as nanoporous adsorbent for removal of diazinon organophosphorus insecticide from aqueous media.* Journal of Dispersion Science and Technology, 2019.

30. Carson, F., et al., *Framework isomerism in vanadium metal–organic frameworks: MIL-88B (V) and MIL-101 (V).* Crystal growth & design, 2013. **13**(11): p. 5036-5044.

31. Liao, M., et al., *A Deep-Cycle Aqueous Zinc-Ion Battery Containing an Oxygen-Deficient Vanadium Oxide Cathode.* Angew Chem Int Ed Engl, 2020. **59**(6): p. 2273-2278.

32. Racik, K.M., et al., *Enhanced electrochemical performance of MnO_2/NiO nanocomposite for supercapacitor electrode with excellent cycling stability.* Journal of Materials Science: Materials in Electronics, 2019. **30**(5): p. 5222-5232.

33. Jiang, H.-L., et al., *From Metal–Organic Framework to Nanoporous Carbon: Toward a Very High Surface Area and Hydrogen Uptake.* Journal of the American Chemical Society, 2011. **133**(31): p. 11854-11857.

34. Pradeeswari, K., et al., *Effect of cerium on electrochemical properties of V_2O_5 nanoparticles synthesized via non-aqueous sol-gel technique.* Ionics, 2020. **26**(2): p. 905-912.

35. Li, W., et al., *Uncoupled surface spin induced exchange bias in α-MnO_2 nanowires.* Scientific Reports, 2014. **4**(1): p. 1-7.

36. Férey, G., et al., *A chromium terephthalate-based solid with unusually large pore volumes and surface area.* Science, 2005. **309**(5743): p. 2040-2042.

37. Nehru, L., et al., *Electrochemical sensing of serotonin by a modified MnO_2-graphene electrode.* Biosensors, 2020. **10**(4): p. 33.

38. Li, Z., et al., *In situ synthesis rodlike MnO_2/reduced graphene oxide composite as anode materials for Li-ion batteries.* Journal of Materials Science: Materials in Electronics, 2017. **28**(23): p. 18099-18105.

39. Khamsanga, S., et al., *MnO2 Heterostructure on Carbon Nanotubes as Cathode Material for Aqueous Zinc-Ion Batteries.* International Journal of Molecular Sciences, 2020. **21**(13): p. 4689.

40. Liu, X., et al., *Zeolitic imidazolate frameworks as Zn^{2+} modulation layers to enable dendrite-free Zn anodes.* Advanced Science, 2020. **7**(21): p. 2002173.